Structural analysis of heater rods with different groove shapes under pressurized conditions

Jihun Kim[a], SeHyeon Park[b], Sungjin Kwon[c], HangJin Jo[a,b*]
[a]*Department of Mechanical Engineering, POSTECH, Pohang, Republic of Korea*
[b]*Division of Advanced Nuclear Engineering, POSTECH, Pohang, Republic of Korea*
[c]*National Fusion Research Institute, Daejeon 34133, Republic of Korea*

[*]*Corresponding author: jhj04@postech.ac.kr*

***Keywords :** heater rods, groove geometry, stress concentration, pressure-induced stress

1. Introduction

In critical heat flux (CHF) experiments conducted under low and high pressure conditions, accurate wall temperature measurement and the structural integrity of heater rods are essential for CHF determination [1]. Conventional CHF experiments typically rely on thermocouples installed near the heater rod outlet, where CHF is expected to occur under uniform heat flux conditions [2-3]. However, thermocouples provide only discrete temperature measurements, making it difficult to detect localized temperature increases at arbitrary axial locations along the heater rod.

To overcome this limitation, distributed optical fiber sensors (OFS) have been introduced to provide high spatial resolution monitoring along the entire heated length [4-5]. While this allows for early detection of CHF initiation, the installation of OFS requires machining grooves into the heater rod surface, which alters its structural geometry. Therefore, quantitative evaluation of stress distribution and structural response associated with these groove geometries is necessary to ensure structural integrity under external pressure conditions.

In this study, three-dimensional finite element analysis (FEA) was performed on Inconel 600 heater rods with three different groove geometries to evaluate stress distribution under external pressure. Stress concentration at the groove notch and axial strain at the OFS attachment location were evaluated for each geometry. Based on these results, the groove geometry with the lowest stress concentration and axial strain was selected for OFS installation.

2. Methods

2.1. Heater Rods and Groove Design

Fig. 1 shows the configuration of the directly heated heater rod and its geometric parameters for OFS installation. As shown in Fig. 1(a), the heater rod consists of an Inconel 600 sheath with copper electrodes attached to both ends. The internal cavity of the sheath is filled with alumina, which acts as an electrical insulator. When electrical current is applied through the copper electrodes, resistive heating occurs in the Inconel 600 sheath. To enable continuous axial temperature measurement using the OFS, grooves are machined on the outer surface of the Inconel 600 sheath. Fig. 1(b) presents the geometric parameters of the Inconel 600 sheath. The outer diameter (OD), inner diameter (ID), and wall thickness (t) are 9.5 mm, 8.5 mm, and 0.5 mm, respectively.

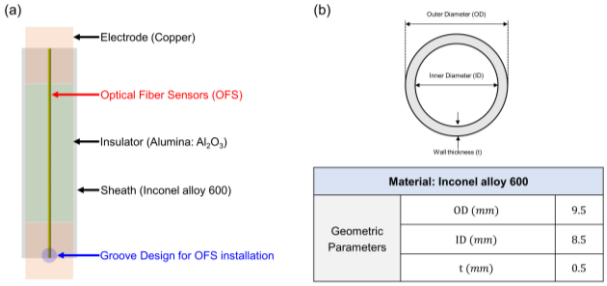

Material: Inconel alloy 600		
Geometric Parameters	OD (*mm*)	9.5
	ID (*mm*)	8.5
	t (*mm*)	0.5

Fig. 1. Heater rod configuration for optical fiber sensor (OFS) installation (a) directly heated heater rod assembly, (b) geometry of Inconel 600 sheath (OD: 9.5 mm, ID: 8.5 mm, t: 0.5 mm)

Fig. 2 shows the geometric parameters of the groove geometries machined on the outer surface of the Inconel 600 sheath for optical fiber sensor (OFS) installation. The following groove geometries were investigated: V-shaped, trapezoidal, and rectangular grooves.

Dimensionless Geometric Parameters	λ (Taper ratio) $= \frac{W_b}{W_t} = \frac{\text{bottom width}}{\text{top width}}$
	AR (Aspect ratio) $= \frac{h}{W_t} = \frac{\text{height}}{\text{top width}}$

	V-Groove	Trapezoidal Groove	Rectangular Groove
		W_t, h, W_b	
W_t [*mm*]	0.195		
W_b [*mm*]	0	0.0975	0.195
h [*mm*]	0.195		
λ	0	0.5	1
AR	1		

Fig. 2. Groove designs and dimensionless parameters for optical fiber sensor (OFS) installation, including groove width (Wt, Wb), depth (h), taper ratio (λ), and aspect ratio (AR) for V-groove, trapezoidal groove, and rectangular groove

Dimensionless geometric parameters were defined to characterize the groove shapes. The taper ratio (λ) was defined as the ratio of the bottom width (Wb) to the top width (Wt), while the aspect ratio (AR) was defined as the ratio of the groove depth (h) to the top width (Wt). For all groove geometries, Wt and h were fixed at 0.195 mm, resulting in an aspect ratio of 1. The bottom width (Wb) was set to 0 mm, 0.0975 mm, and 0.195 mm for the V-shaped, trapezoidal, and rectangular grooves, respectively. The corresponding taper ratios (λ) were 0, 0.5, and 1.

Figs. 3(a)-(c) show the three-dimensional CAD geometries of the heater rods with different groove shapes used for finite element analysis (FEA). The geometries were modeled in ANSYS DesignModeler (ANSYS Inc., Canonsburg, PA, USA) and subsequently analyzed using ANSYS Mechanical.

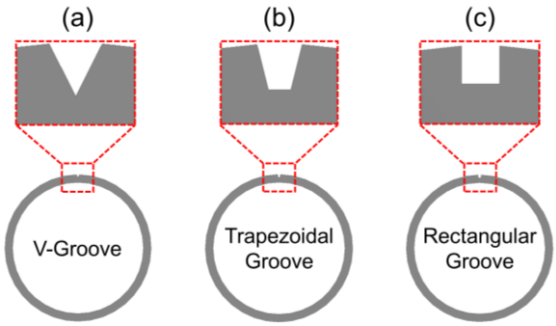

Fig. 3. 3D CAD geometries of groove configurations for the Inconel 600 sheath: (a) V-groove, (b) trapezoidal groove, and (c) rectangular groove

2.2. Material and Boundary Conditions

The mechanical properties of Inconel 600 used for OFS installation are listed in Table I. For the finite element analysis (FEA), Young's modulus and Poisson's ratio were set to 214 GPa and 0.324, respectively. The yield strength and ultimate tensile strength, which were 310 MPa and 655 MPa, respectively, served as reference values for evaluating the stress distribution results. These material properties were selected based on the manufacturer's datasheet.

Table I: Mechanical properties of Inconel 600

Mechanical Properties (Inconel alloy 600)	Young's Modulus (GPa)	214
	Poisson's Ratio	0.324
	Yield Strength (MPa)	310
	Ultimate Tensile Strength (MPa)	655

Fig. 4 presents the boundary conditions applied for the structural analysis under external pressure for different groove geometries. At the cross-section located at Z = 0 mm, a remote displacement was applied with all translational displacements (X, Y, Z) set to 0 mm and all rotational degrees of freedom (X, Y, Z) set to 0°, resulting in a fully constrained condition. At the cross-section located at Z = 300 mm, a remote displacement was also applied with translational displacements in the X and Y directions and all rotational degrees of freedom fixed, while the axial displacement in the Z direction was left free to allow for axial deformation. External pressure was applied uniformly in the normal direction on the outer surface of the Inconel 600 sheath.

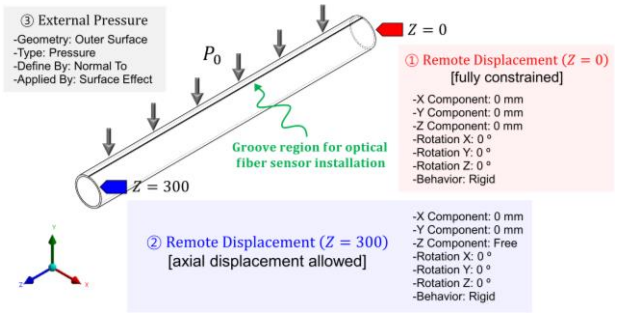

Fig. 4. Boundary conditions for the Inconel 600 sheath under external pressure

3. Results

3.1. Stress Distribution

Fig. 5 shows the stress distribution under an external pressure of 10 MPa applied to the outer surface of the Inconel 600 sheath. To minimize the influence of boundary conditions, the stress distributions were evaluated at the cross-section located at Z = 150 mm, which corresponds to the midpoint between the constrained boundaries at Z = 0 mm and Z = 300 mm.

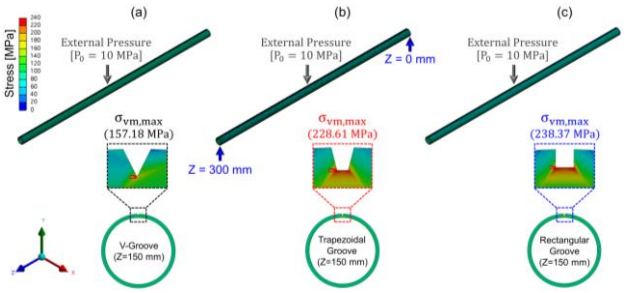

Fig. 5. Stress distribution under external pressure for different groove geometries (a) V-groove, (b) trapezoidal groove, and (c) rectangular groove

Fig. 5(a) presents the stress distribution of the V-groove, where the maximum stress of 157.18 MPa occurred at the groove notch. For the trapezoidal groove shown in Fig. 5(b), the maximum stress was 228.61 MPa, while the rectangular groove showed the highest stress of 238.37 MPa in Fig. 5(c). In all geometries, the highest stress concentration was observed at the groove notch. The V-groove exhibited the lowest maximum stress among the three configurations.

3.2. Maximum Stress under External Pressure

Fig. 6 compares the maximum von Mises stress for different groove geometries as the external pressure increases from 0 to 25 MPa. The rectangular groove exhibited the highest von Mises stress over the entire pressure range, followed by the trapezoidal groove, while the V-groove showed the lowest stress. Compared to the yield strength of Inconel 600 (310 MPa), the rectangular and trapezoidal grooves exceeded the yield limit at an external pressure of approximately 14 MPa. In contrast, the V-groove reached the yield strength at a higher pressure of approximately 20 MPa. For all groove geometries, the maximum stress remained below the ultimate tensile strength (655 MPa) over the entire pressure range. These results indicate that the V-groove provides improved structural integrity by reducing stress concentration compared to the other geometries.

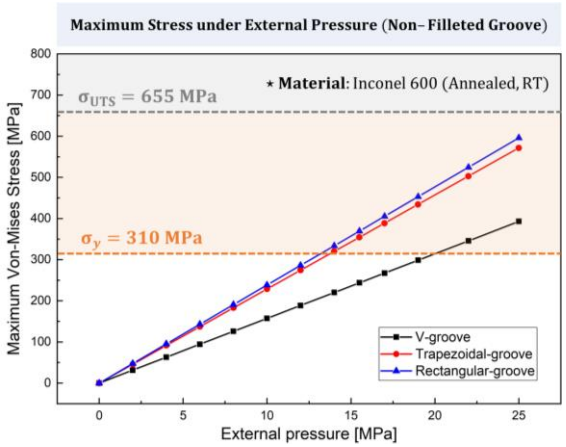

Fig. 6. Comparison of maximum von Mises stress under external pressure for different groove configurations

Fig. 7 shows the maximum von Mises stress for the groove geometries with a fillet radius of 0.01 mm under external pressure ranging from 0 to 25 MPa.

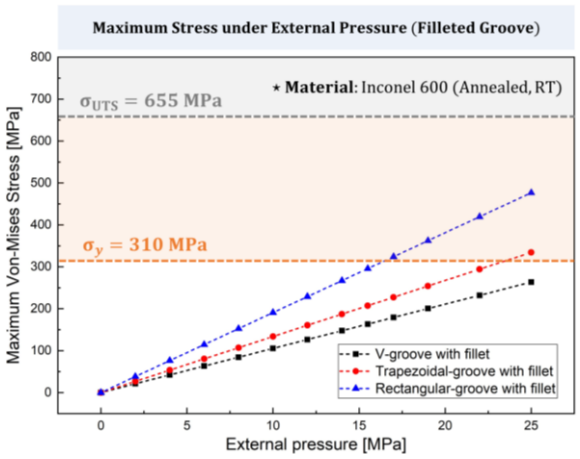

Fig. 7. Maximum von Mises stress at the groove notch for filleted V-groove, trapezoidal groove, and rectangular groove

In the absence of a fillet, stress concentration occurred at the groove notch for all geometries, and maximum von Mises stress exceeded the yield strength at an external pressure of 25 MPa. To mitigate this, a 0.01 mm fillet radius was applied to each groove geometry, and the maximum von Mises stress was evaluated under identical external pressure conditions. For the rectangular groove with a fillet, the yield strength was reached at an external pressure of approximately 17 MPa, while the trapezoidal groove reached the yield strength at approximately 23 MPa. In contrast, the V-groove with a fillet remained below the yield strength over the entire pressure range. These results indicate that the V-groove with a fillet radius of 0.01 mm provides the most favorable structural integrity for OFS installation due to reduced stress concentration at the groove notch.

3.3. Axial Strain at OFS Location

Fig. 8 presents the length-averaged axial strain at the OFS installation location for the groove geometries with a 0.01 mm fillet radius under external pressure. The axial strain was evaluated as a function of external pressure to assess the structural response at the OFS attachment point. Among the three geometries, the filleted V-groove exhibited the lowest axial strain under identical pressure conditions. This result indicates that the filleted V-groove is less susceptible to pressure-induced deformation. Consequently, the filleted V-groove is the most suitable configuration for OFS installation, as it minimizes extraneous pressure-induced strain, thereby enabling more accurate temperature measurement based primarily on thermal expansion.

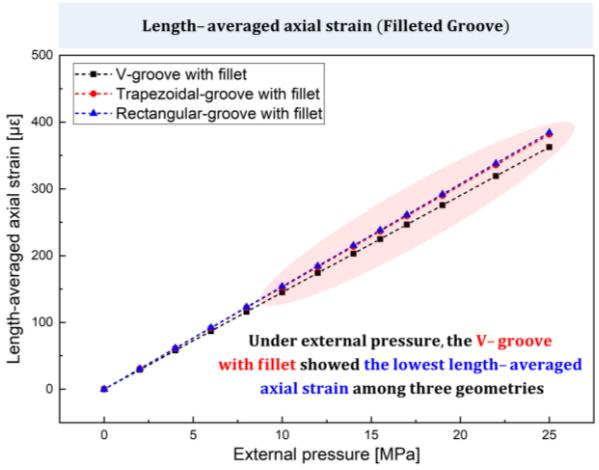

Fig. 8. Length-averaged axial strain for filleted V-groove, trapezoidal groove, and rectangular groove

4. Conclusions

In this study, a structural analysis was performed to evaluate heater rods with different groove geometries for optical fiber sensor (OFS) installation under external pressure. Stress concentration occurred at the groove notch for all geometries, and the V-groove exhibited the lowest stress levels. With the application of a 0.01 mm fillet radius, the V-groove maintained stress levels below the yield strength over the pressure range between 0 and 25 MPa. Furthermore, the filleted V-groove showed the lowest axial strain at the OFS installation location, effectively minimizing extraneous pressure-induced interference. Consequently, the filleted V-groove was identified as the most suitable geometry for reliable OFS operation under pressurized conditions.

5. Acknowledgement

This research was supported by an internal project (development of critical heat flux measurement technique using optical fiber temperature sensor) grant funded by KEPCO Nuclear Fuel Co., Ltd., Republic of Korea, and by the National Research Council of Science & Technology (NST) grant funded by the Korea government (MSIT) (No. GTL25031-000).

REFERENCES

[1] Chen, Sen, et al. "An experimental study of the CHF in a square channel with non-uniformly heated rod under low pressure and low flow conditions." *Nuclear Engineering and Technology* 57.4 (2025): 103284.
[2] Kim, Geon-Woo, et al. "Critical heat flux characteristics of flow boiling on a heater rod under inclined and rolling conditions." *International Journal of Heat and Mass Transfer* 189 (2022): 122670.
[3] Lyons, Kathleen, Donghwi Lee, and Mark Anderson. "Experimental study for critical heat flux in 2x2 rod bundles at high pressure conditions." *Nuclear Engineering and Design* 365 (2020): 110730.
[4] Hyer, Holden C., Dominic R. Giuliano, and Christian M. Petrie. "Toward local core outlet temperature monitoring in gas-cooled nuclear reactors using distributed fiber-optic temperature sensors." *Applied Thermal Engineering* 230 (2023): 120847.
[5] Nam, Hyeon Taek, et al. "State-of-the-art optical fiber temperature measurement on a micro-pillar interfacial surface during flow boiling heat transfer." *Energy* (2026): 139978.